Mem. S.A.It. Suppl. Vol. 13, 97

Memorie della
Supplementi

MHD modeling of supernova remnants expanding through inhomogeneous interstellar medium

S. Orlando[1,2], F. Bocchino[1,2], M. Miceli[2,1], F. Reale[3,1,2], and G. Peres[3,1,2]

[1] Istituto Nazionale di Astrofisica – Osservatorio Astronomico di Palermo, Piazza del Parlamento 1, 90134 Palermo, Italy, e-mail: orlando@astropa.inaf.it
[2] Consorzio COMETA, via Santa Sofia 64, 95123 Catania, Italy
[3] DSFA - Università di Palermo, Piazza del Parlamento 1, 90134 Palermo, Italy

Abstract. We model the expansion of a blast wave of a supernova explosion through a magnetized and inhomogeneous interstellar medium (ISM). The aim is to explore the role of an ambient magnetic field and/or a non-uniform ISM in determining the morphology of supernova remnants (SNRs) as observed in different bands. In particular, we investigate: 1) whether the morphology of bilateral SNRs (BSNRs) observed in the radio band is mainly determined by a non-uniform ISM or by a non-uniform ambient magnetic field and 2) the role of thermal conduction and of non-uniform ISM in determining the morphology and physical characteristics of mixed-morphology (MM) SNRs. We present 3-D hydrodynamic and MHD simulations of a spherical SNR shock propagating through an inhomogeneous ISM. We discuss the origin of the asymmetries observed in BSNRs and of the unexpected morphology observed in MM-SNRs.

Key words. Magnetohydrodynamics (MHD) – Shock waves – ISM: supernova remnants – ISM: magnetic fields

1. Introduction

The interaction of shock waves of supernova remnants (SNRs) with the magnetized and inhomogeneous interstellar medium (ISM) is responsible of the great morphological complexity of SNRs and certainly plays a major role in determining the exchange of mass, momentum, and energy between diffuse hot plasma and dense clouds or clumps (see, for instance, Orlando et al. 2005, 2008). However, the details of the interaction between SNR shock fronts and ISM depend, in principle, on many factors, among which the multiple-phase structure of the medium, its density and temperature, the intensity and direction of the ambient magnetic fields. These factors are not easily determined and this somewhat hampers our detailed understanding of the complex ISM.

We have started a project devoted to study the interaction of SNRs expanding through the magnetized inhomogeneous ISM. The project aims at overcoming some of the limitations found in previous analogous studies and which do not allow an accurate interpretation of the high resolution multi-wavelength observations of middle-aged SNR shell available

Send offprint requests to: S. Orlando

with the last-generation instruments. In this paper, we review our recent results on the study of: 1) the origin of asymmetries observed in the the so-called bilateral supernova remnants (BSNRs, Kesteven & Caswell 1987; Gaensler 1998; Fulbright & Reynolds 1990) and 2) the role of inhomogeneous ISM and/or thermal conduction in shaping the morphology of metal-rich Mixed-Morphology (MM) SNRs (e.g. Rho & Petre 1998).

2. Bilateral supernova remnants (BSNRs)

The BSNRs are considered a benchmark for the study of large scale SNR-ISM interactions, since no small-scale effect like encounters with ISM clouds seems to be relevant. The BSNRs are characterized by two opposed radio-bright limbs separated by a region of low surface brightness. In general, the remnants appear asymmetric, distorted and elongated with respect to the shape and surface brightness of the two opposed limbs.

Our project has aimed at exploring two main aspects of the nature of BSNRs: how and under which physical conditions do the asymmetries originate in BSNRs? Is the ambient magnetic field or the non-uniform ISM more effective in determining the morphology and the asymmetries of this class of SNRs?

Answering such questions at an adequate level requires detailed physical modeling, high-level numerical implementations and extensive simulations. To this end, we modeled the propagation of a shock generated by an SN explosion in the magnetized non-uniform ISM with detailed numerical MHD simulations (Orlando et al. 2007).

2.1. The model

The shock propagation is modeled by numerically solving the time-dependent ideal MHD equations of mass, momentum, and energy conservation in a 3-D cartesian coordinate system (x, y, z):

$$\frac{\partial \rho}{\partial t} + \nabla \cdot (\rho \mathbf{u}) = 0 \,, \tag{1}$$

$$\frac{\partial \rho \mathbf{u}}{\partial t} + \nabla \cdot (\rho \mathbf{u}\mathbf{u} - \mathbf{B}\mathbf{B}) + \nabla P_* = 0 \,, \tag{2}$$

$$\frac{\partial \rho E}{\partial t} + \nabla \cdot [\mathbf{u}(\rho E + P_*) - \mathbf{B}(\mathbf{u} \cdot \mathbf{B})] = 0 \,, \tag{3}$$

$$\frac{\partial \mathbf{B}}{\partial t} + \nabla \cdot (\mathbf{u}\mathbf{B} - \mathbf{B}\mathbf{u}) = 0 \,, \tag{4}$$

where

$$P_* = P + \frac{B^2}{2} \,, \qquad E = \epsilon + \frac{1}{2}|\mathbf{u}|^2 + \frac{1}{2}\frac{|\mathbf{B}|^2}{\rho} \,,$$

are the total pressure (thermal pressure, P, and magnetic pressure) and the total gas energy (internal energy, ϵ, kinetic energy, and magnetic energy) respectively, t is the time, $\rho = \mu m_H n_{\rm H}$ is the mass density, $\mu = 1.3$ is the mean atomic mass (assuming cosmic abundances), m_H is the mass of the hydrogen atom, $n_{\rm H}$ is the hydrogen number density, $\mathbf{u}$ is the gas velocity, T is the temperature, and $\mathbf{B}$ is the magnetic field. We use the ideal gas law, $P = (\gamma - 1)\rho\epsilon$, where $\gamma = 5/3$ is the adiabatic index. The simulations are performed using the FLASH code (Fryxell et al. 2000), an adaptive mesh refinement multiphysics code for astrophysical plasmas.

As initial conditions, we assumed a spherical remnant with radius $r_{0\rm snr} = 4$ pc and with total energy $E_0 = 1.5 \times 10^{51}$ erg, originating from a progenitor star with mass of 15 $M_{\rm sun}$, and propagating through an unperturbed magnetohydrostatic medium. We followed the expansion of the remnant for 22 kyrs, exploring the space of relevant parameters (see Orlando et al. 2007), and considering two sets of simulations to explore the role of inhomogeneous ISM or non-uniform ambient magnetic field in determining the asymmetries of BSNRs: 1) SNR expanding through a gradient of ambient density with a uniform ambient magnetic field; or 2) SNR expanding through a homogeneous isothermal medium with a gradient of ambient magnetic field strength.

2.2. Results

In all the models examined, we found the typical evolution of adiabatic SNRs expanding

through an organized ambient magnetic field (Orlando et al. 2007; see also Balsara et al. 2001 and references therein): the fast expansion of the shock front with temperatures of a few millions degrees, and the development of Richtmyer-Meshkov (RM) instability, as the forward and reverse shocks progress through the ISM and ejecta, respectively (see Kane et al. 1999). As examples, Fig. 1 shows 2-D sections in the (x, z) plane of the distributions of mass density (upper panel) and of magnetic field strength (lower panel) for a model assuming inhomogeneous medium and uniform magnetic field at $t = 18$ kyrs. The inner shell is dominated by the R-M instability that causes the plasma mixing and the magnetic field amplification.

From the simulations, we synthesized the radio emission from the remnant, assuming that it is only due to synchrotron radiation from relativistic electrons distributed with a power law spectrum $N(E) = KE^{-\zeta}$, where E is the electron energy, $N(E)$ is the number of electrons per unit volume with arbitrary directions of motion and with energies in the interval $[E, E + dE]$, K is the normalization of the electron distribution, and ζ is the power law index. Since K depends on the injection efficiency (the fraction of electrons that move into the cosmic-ray pool), we have considered the main models of acceleration and injection of relativistic electrons discussed in literature (Orlando et al. 2007; see also Fulbright & Reynolds 1990; Ellison et al. 1995; Reynolds 1998; Petruk & Bandiera 2006).

Figure 2 shows the radio emission maps, at a time of 18 kyrs, synthesized from models with a gradient of ambient plasma density (panels A and D) and of ambient **B** field strength (panels B and E). All the models assume quasi-perpendicular particle injection (the isotropic case produces radio maps with similar morphologies and the quasi-parallel case is discussed later) and randomized internal magnetic field. The viewing angle is perpendicular both to the average direction of the unperturbed ambient magnetic field, $\langle \mathbf{B} \rangle$, (direct along the x axis) and to the gradients of density or field strength (direct either

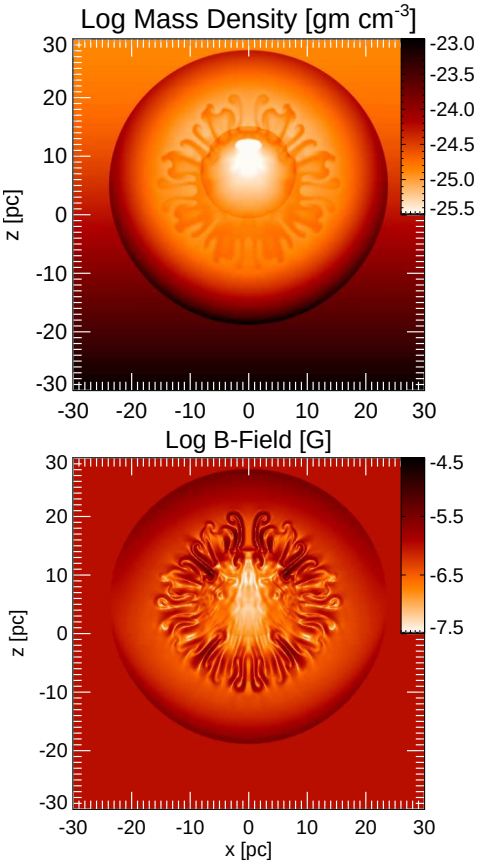

Fig. 1. 2-D sections in the (x, z) plane of the mass density distribution (upper panel), in log scale, and of the distribution of the magnetic-field strength (lower panel), in log scale, for a model assuming inhomogeneous medium and uniform magnetic field, at $t = 18$ kyrs (adapted from Orlando et al. 2007).

along z, panels A and B, or x, panels D and E). The right panels show examples of the radio maps of the SNRs G338.1+04 (panel C, data from Whiteoak & Green 1996) and G296.5+10.0 (panel F, from Gaensler 1998).

We find that asymmetric BSNRs are produced if the line-of-sight is not aligned with the gradient of ambient plasma density or with the gradient of ambient magnetic field strength. BSNRs with two radio limbs of different brightness can be explained if a gradient of ambient density or, most likely, of ambient magnetic field strength is perpendicular to

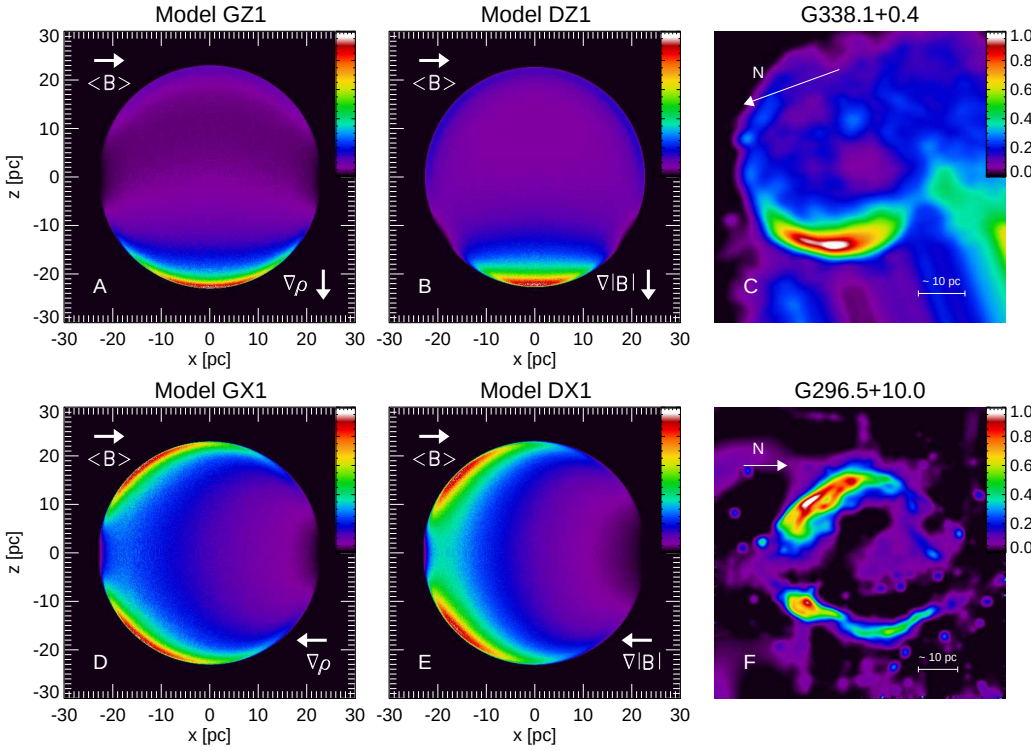

Fig. 2. Synchrotron radio emission (normalized to the maximum of each panel), at t = 18 kyrs, synthesized from models assuming a gradient of ambient plasma density (panels A and D) or of ambient magnetic field strength (panels B and E) when the LoS is aligned with the y axis (adapted from Orlando et al. 2007). All the models assume quasi-perpendicular particle injection. The directions of the average unperturbed ambient magnetic field, $\langle \mathbf{B} \rangle$, and of the plasma density or magnetic field strength gradient, are shown in the upper left and lower right corners of each panel, respectively. The right panels show two examples of radio maps (data adapted from Whiteoak & Green 1996 and Gaensler 1998; the arrows point in the north direction) collected for the SNRs G338.1+0.4 (panel C) and G296.5+10.0 (panel F). The color scale is linear and is given by the bar on the right.

the radio limbs. BSNRs with converging similar radio arcs can be explained if the gradient runs between the two arcs.

3. Mixed-morphology supernova Remnants (MM-SNRs)

MM-SNRs are characterized by a shell-like morphology in the radio band and centrally peaked thermal emission in the X-ray band coming from shocked interstellar medium (e.g. Rho & Petre 1998). A mechanism that is responsible for producing such an unexpected morphology has not yet been uniquely identified. Moreover, Lazendic & Slane (2006) reported that, of 23 MM-SNRs, 10 show evidence for enhanced abundances, thus strongly suggesting the presence of stellar fragments (ejecta) intermixed with hot shocked ISM inside some the MM-SNRs. This was also the case of traditional MM-SNR prototypes like W44 (Shelton et al. 2004), IC443 (Troja et al. 2006) as well as for other MM-SNRs (e.g. MSH 11-61A, Slane et al. 2002).

Traditional models, which neglected the presence of ejecta in the hot core and which assumed spherical symmetry, must therefore be revisited in the light of these new obser-

vational evidences. It seems much more reasonable that MM-SNRs models must be modified to take into account the interaction between the reverse shock and the ejecta in presence of thermal conduction. Moreover, since many MM-SNRs come from core-collapse of massive stars (because the presence of a pulsar), their evolution may be heavily affected by the configuration of the circumstellar medium (CSM) at the time of SN explosion. Wind-blown bubbles may be produced by massive stars in the main sequence, undergoing red super giant (RSG) and Wolf-Rayet phases. The interaction of the forward SNR shock with the shells formed by stellar winds may result in a strong reflected shock driven back into the ejecta, and it is reasonable to assume that the centrally peaked morphology may be the results of these interactions.

Our project aims at a physical understanding of metal-rich MM-SNRs, addressing and overcoming the limitations of previous models. To this end, we have developed a model including a typical scenario for the environment of a core-collapse SN, namely an extended wind-blown bubble created during the red supergiant phase (Orlando et al. in preparation). Moreover, we have synthesized X-ray spectra of SNR inner regions with emission models with variable metallicity, with the aim to assess the role of ejecta material on the detection of a mixture of high and low metallicity plasma (Orlando et al. in preparation).

3.1. The model

We model the blast wave originating from a supernova explosion that propagates into a wind-blown bubble surrounded by a thin dense, cool shell originating from the interaction between the wind of the progenitor star and the surrounding medium. The system is modeled by solving numerically the time-dependent hydrodynamical equations of mass, momentum, and energy conservation (see Eqs. 1-4 with $\mathbf{B} = 0$), taking into account the effects of thermal conduction (including effects of heat flux saturation) and radiative losses. The ejecta material (characterized by high metallicity) in each computational cell are followed using a color tracer, which is initially set to 1 for ejecta material and 0 for CSM/ISM material. The calculations are carried out with the FLASH code (Fryxell et al. 2000), extended with additional computational modules to handle the radiative losses and the thermal conduction (see Orlando et al. 2005 for the details of the implementation).

Our initial condition represents the remnant of a 15 $M_{\rm sun}$ star that exploded about 10^5 yr after the onset of the RSG phase. The initial SNR is modeled as a sphere centered on the origin of the cartesian coordinate system. The total energy of the initial explosion is 10^{51} ergs which is split into kinetic and thermal energy. The ambient medium is modeled as a RSG wind-blown bubble of about 13 pc radius, surrounded by a dense, cool shell. The wind is initialized isothermal with profiles of density derived by Dwarkadas (2005).

3.2. Results

Our simulations have shown that, after the SN explosion, the blast wave travels at high speed inside the bubble, reaching the cavity wall (i.e. the thin shell due to the accumulation of wind swept-up material) after about 2,500 yrs. Unlike the homogeneous case, the blast wave becomes radiative after hitting the cavity wall. The interaction with the dense material of the shell drives a forward shock with temperatures $\sim 10^4$ K and a reverse shock with $T \sim 10^7$ K propagating through the post shock CSM and the ejecta. After $\sim 18,000$ yrs, the latter reaches the center of the remnant, contributing to an increase of density there in subsequent phases. As an example, Fig. 3 shows the 3D spatial distributions of mass density (in log scale) and of ejecta at $t \approx 30,000$ yrs, i.e. during the phase of density increase. During this phase, the reverse shock travels through the ejecta, contributing to concentrate them in the inner regions of the remnant (lower panel of Fig. 3), and playing a crucial role in the spatial distributions of abundances within the remnant.

From the models, we have synthesized the X-ray emission, applying the method described by Orlando et al. (2006) (see also

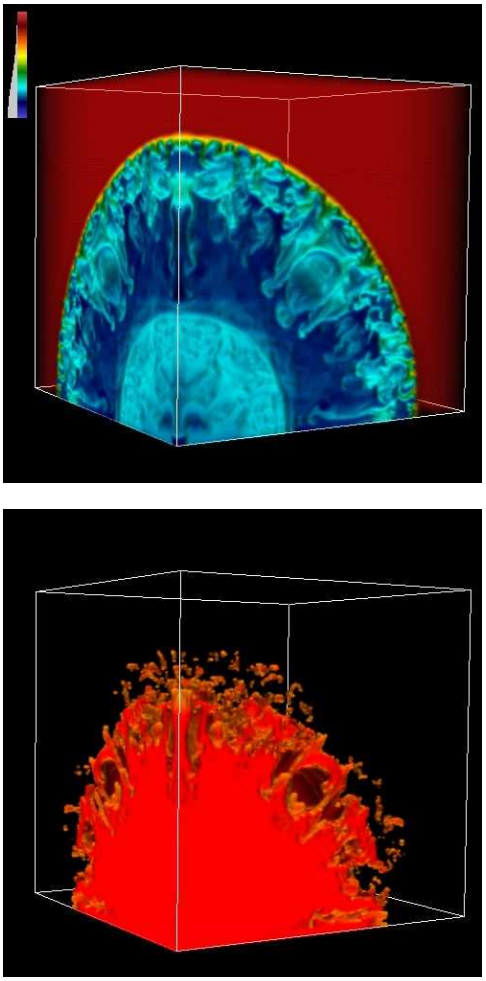

Fig. 3. Spatial distributions of mass density, in log scale, (upper panel) and of ejecta (lower panel) at $t \approx 30,000$ yrs (see text for more details).

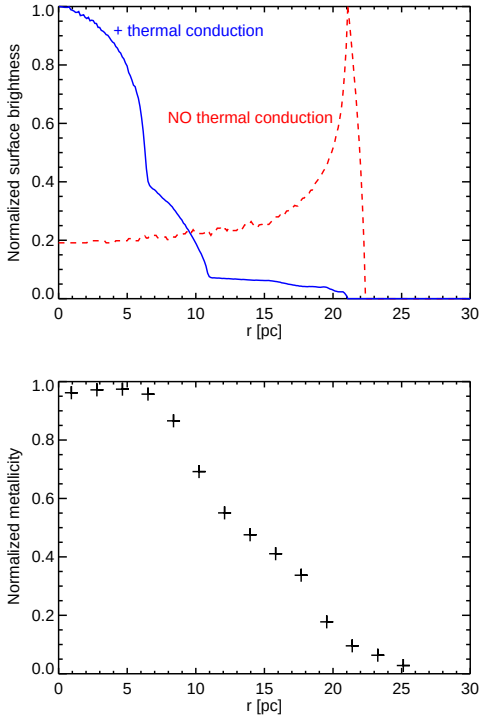

Fig. 4. Upper panel: Radial profile of surface brightness (normalized to the maximum) for models either with (blue line) or without (red) thermal conduction at $t \approx 32,000$ yrs. Lower panel: Radial profile of average metallicity along the line-of-sight normalized to the metallicity of ejecta for the model with thermal conduction at $t \approx 32,000$ yrs.

Miceli et al. 2006). We derived maps of X-ray emission in different phases of the remnant evolution and found that the morphology of the SNR changes with time. During the first phase (i.e. when the reverse shock has not reached yet the center of the remnant), the X-ray emission is maximum just behind the forward shock and the remnant has a shell-like morphology. After the reverse shock has reached the center of the remnant, the X-ray emission is maximum at the center of the remnant and the morphology is centrally bright as observed in MM-SNRs.

We have investigated the role of the thermal conduction by comparing the X-ray emission derived from models calculated with thermal conduction either active or inactive. The upper panel of Fig. 4 shows the radial profile of surface brightness (normalized to the maximum) synthesized from these models at $t \approx 32,000$ yrs. It is evident that the thermal conduction plays a crucial role in determining MM-SNRs.

Finally, we have investigated the radial dependence of metallicity as derived from our models. The lower panel of Fig. 4 shows the radial profile of average metallicity along the line-of-sight normalized to the metallicity of ejecta at $t \approx 32,000$ yrs (i.e. when the remnant has a centrally bright X-ray morphology). We

found that the abundances are highly metallic in the inner part of the remnant and decrease with the radial distance. This is reminiscent of what is observed in many metal-rich MM-SNRs. Our analysis has shown that this feature is due to the reverse shock, confining the ejecta in the inner part of the remnant.

4. Summary and conclusions

In this paper, we have reviewed some results obtained in a project devoted to study the dynamics and energetic of SNRs expanding through the magnetized and inhomogeneous ISM. In particular, we have reported on the study of the origin of asymmetries in BSNRs and on the role of inhomogeneous ISM and of thermal conduction in determining the morphology of MM-SNRs.

We found that asymmetric BSNRs are produced if the line-of-sight is not aligned with the gradient of ambient plasma density or with the gradient of ambient magnetic field strength. Gradients of magnetic field strength are more effective in generating the asymmetries.

As for the MM-SNRs, we found that their morphology is determined by the combined action of thermal conduction. and inhomogeneous CSM in which the blast wave expands. MM-SNRs form in late phases of the evolution, $\approx 30,000$ yrs after the SN. We found enhanced metallicity at the center of the remnant due to ejecta material confined by the reverse shock.

Acknowledgements. The software used in this work was in part developed by the DOE-supported ASC/Alliance Center for Astrophysical Thermonuclear Flashes at the University of Chicago. The simulations were executed at CINECA (Bologna, Italy) in the framework of the INAF-CINECA agreement on "High Performance Computing resources for Astronomy and Astrophysics". This work makes use of results produced by the PI2S2 Project managed by the Consorzio COMETA, a project co-funded by the Italian Ministry of University and Research (MIUR) within the Piano Operativo Nazionale "Ricerca Scientifica, Sviluppo Tecnologico, Alta Formazione" (PON 2000-2006). More information is available at http://www.pi2s2.it and http://www.consorzio-cometa.it. This work was supported by Ministero dell'Istruzione, dell'Università e della Ricerca, by Istituto Nazionale di Astrofisica, and by Agenzia Spaziale Italiana (ASI/INAF I/023/05/0).

References

Balsara, D., Benjamin, R. A., & Cox, D. P. 2001, ApJ, 563, 800
Dwarkadas, V. V. 2005, ApJ, 630, 892
Ellison, D. C., Baring, M. G., & Jones, F. C. 1995, ApJ, 453, 873
Fryxell, B., Olson, K., Ricker, P., et al. 2000, ApJS, 131, 273
Fulbright, M. S. & Reynolds, S. P. 1990, ApJ, 357, 591
Gaensler, B. M. 1998, ApJ, 493, 781
Kane, J., Drake, R. P., & Remington, B. A. 1999, ApJ, 511, 335
Kesteven, M. J. & Caswell, J. L. 1987, A&A, 183, 118
Lazendic, J. S. & Slane, P. O. 2006, ApJ, 647, 350
Miceli, M., Reale, F., Orlando, S., & Bocchino, F. 2006, A&A, 458, 213
Orlando, S. Bocchino, F., Peres, G., Reale, F., Plewa, T., & Rosner, R. 2006, A&A, 457, 545
Orlando, S., Bocchino, F., Reale, F., Peres, G., & Pagano, P. 2008, ApJ, 678, 274
Orlando, S., Bocchino, F., Reale, F., Peres, G., & Petruk, O. 2007, A&A, 470, 927
Orlando, S., Peres, G., Reale, F., et al. 2005, A&A, 444, 505
Petruk, O. & Bandiera, R. 2006, J. Phys. Studies, 10, 66
Reynolds, S. P. 1998, ApJ, 493, 375
Rho, J. & Petre, R. 1998, ApJ, 503, L167+
Shelton, R. L., Kuntz, K. D., & Petre, R. 2004, ApJ, 615, 275
Slane, P., Smith, R. K., Hughes, J. P., & Petre, R. 2002, ApJ, 564, 284
Troja, E., Bocchino, F., & Reale, F. 2006, ApJ, 649, 258
Whiteoak, J. B. Z. & Green, A. J. 1996, A&AS, 118, 329